Draft version May 14, 2015
Preprint typeset using LaTeX style emulateapj v. 01/23/15

SUPERMASSIVE BLACK HOLE AND HOST BULGE AFFAIRS II. THE RED AND BLUE SEQUENCE IN THE $M_{\rm BH} - M_{*,\rm SPH}$ DIAGRAM.

G. A. D. Savorgnan and A. W. Graham
Centre for Astrophysics and Supercomputing, Swinburne University of Technology, Hawthorn, Victoria 3122, Australia.

A. Marconi
Dipartimento di Fisica e Astronomia, Universitá di Firenze, via G. Sansone 1, I-50019 Sesto Fiorentino, Firenze, Italy.

and

E. Sani
European Southern Observatory, Alonso de Cordova, Vitacura 3107, Santiago, Chile.

Draft version May 14, 2015

ABSTRACT

In our first paper, we performed a detailed (i.e. bulges, disks, bars, spiral arms, rings, haloes, nuclei, cores, etc.) decomposition of 66 galaxies, with directly measured black hole masses, that had been imaged at 3.6 μm with *Spitzer*. Our sample is the largest to date and, for the first time, the decompositions were checked to be consistent with the galaxy kinematics. Here we present correlations between the black hole mass, $M_{\rm BH}$, and the host spheroid (and galaxy) luminosity, $L_{\rm sph}$ (and $L_{\rm gal}$), and also stellar mass, $M_{*,\rm sph}$. Most previous studies have used galaxy samples that were overwhelmingly dominated by high-mass, early-type objects. Instead, our sample includes 17 spiral galaxies, half of which have $M_{\rm BH} < 10^7$ M$_\odot$, and allows us to better investigate the poorly studied low-mass end of the $M_{\rm BH} - M_{*,\rm sph}$ correlation. The bulges of early-type (E + S0) galaxies follow $M_{\rm BH} \propto M_{*,\rm sph}^{1.04\pm0.10}$, consistent with a dry-merging formation scenario, and define a tight *red sequence* with intrinsic scatter $\epsilon_{(Y|X)} = 0.43 \pm 0.06$ dex. On the other hand, the bulges of late-type (Sp) galaxies define a much steeper *blue sequence*, with $M_{\rm BH} \propto M_{*,\rm sph}^{2-3}$, indicating that gas-rich processes feed the black hole more efficiently than the host bulge as they grow. We additionally report that: i) Sérsic galaxies follow $M_{\rm BH} \propto M_{*,\rm sph}^{1.48\pm0.20}$, a less steep sequence than previously reported; ii) bulges with Sérsic index $n_{\rm sph} < 2$, argued by some to be pseudo-bulges, are not offset to lower $M_{\rm BH}$ from the correlation defined by bulges with $n_{\rm sph} > 2$; and iii) $L_{\rm sph}$ and $L_{\rm gal}$ correlate equally well with $M_{\rm BH}$, in terms of intrinsic scatter, only for early-type galaxies; once reasonable numbers of spiral galaxies are included, the correlation with $L_{\rm sph}$ is better than that with $L_{\rm gal}$. **241 words**

Subject headings: **keywords**

1. INTRODUCTION

A quarter of a century ago, Dressler (1989) foresaw a "rough scaling of black hole mass with the mass of the spheroidal component" of galaxies, as suggested by the sequence of five galaxies (M87, M104, M31, M32 and the Milky Way). Yee (1992) also announced a relation between what was effectively black hole mass and galaxy mass for high-luminosity, bulge-dominated early-type galaxies. This "rough scaling" was a premature version of the nowadays popular correlation between black hole mass, $M_{\rm BH}$, and host spheroid luminosity, $L_{\rm sph}$, and also host spheroid mass, $M_{\rm sph}$ (Kormendy & Richstone 1995; Magorrian et al. 1998; Marconi & Hunt 2003; Häring & Rix 2004). These early studies were dominated by high-mass, early-type galaxies, for which they reported a quasi-linear $M_{\rm BH} - M_{\rm sph}$ relation, consistent with a dry-merging formation scenario which would build and maintain a linear scaling. Subsequent studies of the $M_{\rm BH} - L_{\rm sph}$ and $M_{\rm BH} - M_{\rm sph}$ diagrams (Ferrarese & Ford 2005; Lauer et al. 2007a; Graham 2007; Gültekin et al. 2009; Sani et al. 2011; Beifiori et al. 2012; Erwin & Gadotti 2012; Vika et al. 2012; van den Bosch et al. 2012; McConnell & Ma 2013; Kormendy & Ho 2013) continued to use galaxy samples dominated by high-mass, early-type systems having $M_{\rm BH} \gtrsim 0.5\times10^8$ M$_\odot$, and recovered a near-linear relation. However, the consensus about a linear $M_{\rm BH} - M_{\rm sph}$ correlation was not unanimous. Some studies reported a slope steeper than one, or noticed that low-mass spheroids were offset to the lower right of the relation traced by their high-mass counterparts (Laor 1998; Wandel 1999; Laor 2001; Ryan et al. 2007). Graham (2012), Graham & Scott (2013) and Scott et al. (2013) found two distinct trends in the $M_{\rm BH} - L_{\rm sph}$ and $M_{\rm BH} - M_{\rm sph}$ diagrams, i.e. a linear and a quadratic correlation at the high- and low-mass end, respectively. Those readers interested in an extensive review about the early discovery and successive improvements of these correlations should consult Graham (2015b).

Recently, Läsker et al. (2014a,b) derived 2.2 μm bulge luminosities for 35 galaxies (among which only 4 were classified as spiral galaxies), and reported a slope below unity for their $M_{\rm BH} - L_{\rm sph}$ relation. They also claimed that the black hole mass correlates equally well with the total galaxy luminosity as it does with the bulge lumi-

gsavorgn@astro.swin.edu.au

nosity. Now we roughly double the sample.

The $M_{\rm BH}-L_{\rm sph}$ relation can be predicted from other two correlations that involve the bulge stellar velocity dispersion, σ. The first of these two is the $M_{\rm BH}-\sigma$ relation (Ferrarese & Merritt 2000; Gebhardt et al. 2000), which can be described with a single power-law ($M_{\rm BH}\propto\sigma^{5-6}$) over a wide range in velocity dispersion ($70-350$ km s^{-1}, e.g. Graham et al. 2011; McConnell et al. 2011; Graham & Scott 2013). The second is the $L_{\rm sph}-\sigma$ relation, which has long been known to be a "double power-law", with $L_{\rm sph}\propto\sigma^{5-6}$ at the luminous end (Schechter 1980; Malumuth & Kirshner 1981; von der Linden et al. 2007; Lauer et al. 2007b; Liu et al. 2008), and $L_{\rm sph}\propto\sigma^2$ at intermediate and faint luminosities (Davies et al. 1983; Held et al. 1992; Matković & Guzmán 2005; de Rijcke et al. 2005; Balcells et al. 2007; Chilingarian et al. 2008; Forbes et al. 2008; Cody et al. 2009; Tortora et al. 2009; Kourkchi et al. 2012). The change in slope of the $L_{\rm sph}-\sigma$ relation occurs at $M_B\approx-20.5$ mag, corresponding to $\sigma\approx200$ km s^{-1}. The $M_{\rm BH}-L_{\rm sph}$ relation should therefore be better described by a "broken", rather than a single, power-law, with $M_{\rm BH}\propto L_{\rm sph}^{2.5}$ at the low-luminosity end, and $M_{\rm BH}\propto L_{\rm sph}^{1}$ at the high-luminosity end. Due to the scatter in the $M_{\rm BH}-L_{\rm sph}$ (or $M_{\rm BH}-M_{\rm sph}$) diagram, studies that have not sufficiently probed below $M_{\rm BH}\approx10^7$ M$_\odot$ can easily miss the change in slope occuring at $M_{\rm BH}\approx10^{(8\pm1)}$ M$_\odot$, and erroneously recover a single log-linear relation.

When Graham (2012) pointed out this overlooked inconsistency between these linear and bent relations, he identified two different populations of galaxies, namely the core-Sérsic (Graham et al. 2003; Trujillo et al. 2004) and Sérsic spheroids[1], and attributed the change in slope (from super-quadratic to linear) to their different formation mechanisms. In this scenario, core-Sérsic spheroids are built in additive dry merger events, where the black hole and the bulge grow at the same pace, increasing their mass in lock steps ($M_{\rm BH}\propto L_{\rm sph}^{1}$), whereas Sérsic spheroids originate from gas-rich processes, in which the mass of the black hole increases more rapidly than the mass of its host spheroid ($M_{\rm BH}\propto L_{\rm sph}^{2.5}$).

Graham & Scott (2013, hereafter GS13) and Scott et al. (2013) presented double power-law linear regressions for Sérsic and core-Sérsic spheroids in the $M_{\rm BH}-L_{\rm sph}$ and $M_{\rm BH}-M_{*,\rm sph}$ (spheroid stellar mass) diagrams, probing down to $M_{\rm BH}\approx10^6$ M$_\odot$. To obtain their dust-corrected *bulge* magnitudes, they did not perform bulge/disc decompositions, but instead they converted $B-$band and K_S-band observed, total *galaxy* magnitudes using a mean statistical bulge-to-total ratio based on each object's morphological type and disc inclination[2]. These mean statistical bulge-to-total ratios were obtained from the results of literature two-component (Sérsic-bulge/exponential-disk) decompositions.

Several recent papers (Jiang et al. 2011, 2013; Mathur et al. 2012; Reines et al. 2013) claimed an offset at the low-mass end of the $M_{\rm BH}-M_{*,\rm sph}$ diagram, such that the black hole mass is lower than expected from the near-linear correlation traced by the high-mass, early-type spheroids. However, Graham & Scott (2013) showed that the low-mass spheroids ($10^{8.5}\lesssim M_{*,\rm sph}/{\rm M}_\odot\lesssim10^{10.5}$) are not randomly offset from such near-linear correlation, but follow the steeper relation traced by the Sérsic spheroids. Using bulge/disk decomposition data from Jiang et al. (2011), Graham & Scott (2015) derived the host spheroid masses and showed that the steeper $M_{\rm BH}-M_{*,\rm sph}$ extends to these spheroids with even lower black hole masses ($10^5\lesssim M_{*,\rm sph}/{\rm M}_\odot\lesssim2\times10^6$), and a more detailed analysis will be presented in Graham et al. (2015, *in preparation*).

Here we investigate substructure in the $M_{\rm BH}-L_{\rm sph}$ and $M_{\rm BH}-M_{*,\rm sph}$ diagrams using state-of-the-art galaxy decompositions (Savorgnan & Graham 2015, hereafter *Paper I*) for the largest sample of galaxies with directly measured black hole masses. Our galaxies are large and nearby, which allows us to perform accurate multicomponent decompositions (instead of simple bulge/disk decompositions). Our decompositions were obtained from 3.6 μm *Spitzer* satellite imagery, which is an excellent proxy for the stellar mass, superior to the $K-$band (Sheth et al. 2010, and references therein). Nine of our galaxies have $M_{\rm BH}\lesssim10^7$ M$_\odot$, which allows us to constrain the slope of the correlation at the low-mass end. In addition to this, our galaxy sample includes 17 spiral galaxies, representing a notable improvement over past studies dominated by early-type systems. In a forthcoming paper, we will explore the relation between the black hole mass and the bulge dynamical mass, $M_{\rm dyn,sph}\propto R_{\rm e}\sigma^2$, and address the issue of a black hole fundamental plane. **This paper is structured as follows...**

2. DATA

Our galaxy sample (see Table 1) consists of 66 objects for which a dynamical measurement of the black hole mass had been reported in the literature (by GS13 or Rusli et al. 2013) at the time that we started this project, and for which we were able to obtain useful spheroid parameters from 3.6 μm *Spitzer* satellite imagery. Spheroid magnitudes were derived from our state-of-the-art galaxy decompositions, which take into account bulges, disks, spiral arms, bars, rings, haloes, extended or unresolved nuclear sources and partially depleted cores. Kinematical information (Emsellem et al. 2011; Scott et al. 2014; Arnold et al. 2014) was used to confirm the presence of rotationally supported disk components in most early-type galaxies, and to identify their extent (intermediate-scale disks, that are fully embedded in the bulge, or large-scale disks, that encase the bulge and dominate the light at large radii). *Paper I* presents the dataset used here, including details about the data reduction process and the galaxy modelling technique that we developed. It also

[1] Core-Sérsic spheroids have partially depleted cores relative to their outer Sérsic light profile, whereas Sérsic spheroids have no central deficit of stars. While core-Sérsic spheroids are also "core galaxies", as given by the Nuker definition (Lauer et al. 2007b), it should be noted that ∼20% of "core galaxies" are not core-Sérsic spheroids (Dullo & Graham 2014, their Appendix A.2), i.e. do not have depleted cores. The change in slope of the $L_{\rm sph}-\sigma$ relation corresponds to the division between core-Sérsic and Sérsic spheroids (e.g. Graham & Guzmán 2003).

[2] While this resulted in individual bulge magnitudes not being exactly correct, their large sample size allowed them to obtain a reasonable $M_{\rm BH}-L_{\rm sph}$ relation for the ensemble.

discusses how we estimated the uncertainties[3] on the bulge magnitudes, and presents the individual 66 galaxy decompositions, along with a comparison and discussion of past decompositions.

Bulge luminosities[4] (Table 1) from *Paper I* were converted into stellar masses using a constant 3.6 μm mass-to-light ratio, $\Gamma_{3.6} = 0.6$ (Meidt et al. 2014). We additionally explored a more sophisticated way to compute mass-to-light ratios, using the color-$\Gamma_{3.6}$ relation published by Meidt et al. (2014, their equation 4), which allows one to estimate $\Gamma_{3.6}$ of a galaxy from its $[3.6]-[4.5]$ color. Individual $[3.6]-[4.5]$ colors[5] were taken from Peletier et al. (2012, column 8 of their Table 1) when available for our galaxies, or were estimated from the bulge stellar velocity dispersion, σ, using the color-σ relation presented by Peletier et al. (2012, their Figure 6). We found that the range in $[3.6]-[4.5]$ color is small (0.06 mag), and thus the range in $\Gamma_{3.6}$ is also small (0.04). After checking that using a single $\Gamma_{3.6} = 0.6$, independent of $[3.6]-[4.5]$ color, does not significantly affect the results of our analysis, we decided to use individual, color-dependent mass-to-light ratios.

For each galaxy, the total luminosity (or galaxy luminosity, $L_{\rm gal}$) is the sum of the luminosities of all its sub-components. Due to the complexity of their modelling, four galaxies (see Table 1, column 7) had their galaxy luminosities underestimated[6], which are given here as lower limits. Following GS13, we assumed a fixed uncertainty (0.25 mag) for the absolute galaxy magnitude $MAG_{\rm gal}$.

The morphological classification (E = elliptical; E/S0 = elliptical/lenticular; S0 = lenticular; S0/Sp = lenticular/spiral; Sp = spiral; and merger) follows from the galaxy models presented in *Paper I*. Throughout this paper, we will refer to early-type galaxies (E+S0) and late-type galaxies (Sp). Two galaxies classified as E/S0 are obviously included in the early-type bin, whereas two galaxies classified as S0/Sp or another two classified as mergers are included in neither the early- nor the late-type bin.

The Sérsic/core-Sérsic classification presented in this work comes from the compilation of Savorgnan & Graham (2015), who identified partially depleted cores according to the same criteria used by GS13. When no high-resolution image analysis was available from the literature, they inferred the presence of a partially depleted core based on the stellar velocity dispersion: a galaxy is classified as core-Sérsic if $\sigma > 270$ km s^{-1}, or as Sérsic if $\sigma < 166$ km s^{-1}. Galaxies with velocity dispersions between these bands had high-resolution images available.

[3] By comparing, for each of our galaxies, the measurements of the bulge magnitude obtained by different authors with that obtained by us, we estimated the uncertainties on the bulge magnitudes, in effect taking into account systematic errors. Systematic errors include incorrect sky subtraction, inaccurate masking of contaminating sources, imprecise description of the PSF, erroneous choice of model components (for example, when failing to identify a galaxy subcomponent and thus omitting it in the model, or when describing a galaxy sub-component with an inadequate function), the radial extent of the surface brightness profile and one's sampling of this. Most of these factors are not included in popular 2D fitting codes which report only the random errors associated with their fitted parameters. In fact, when performing multi-component decomposition of high signal-to-noise images of nearby – therefore well spatially resolved – galaxies, errors are dominated by systematics rather than Poisson noise.

[4] Following Sani et al. (2011), absolute luminosities were calculated assuming a 3.6 μm solar absolute magnitude of 3.25 mag.

[5] These are integrated $[3.6]-[4.5]$ colors, measured in a circular aperture within each galaxy's effective radius.

[6] These four cases are discussed in *Paper I*.

3. ANALYSIS

We performed a linear regression analysis of the $M_{\rm BH}-L_{\rm gal}$ (see Table 2), $M_{\rm BH}-L_{\rm sph}$ (see Table 3) and $M_{\rm BH}-M_{*,\rm sph}$ (see Table 4) data, using the BCES code from Akritas & Bershady (1996). We also repeated the analysis using both the FITEXY routine (Press et al. 1992), as modified by Tremaine et al. (2002), and the Bayesian estimator `linmix_err` (Kelly 2007). All of these three linear regression routines account for the intrinsic scatter, but only the last two allow one to quantify it. We report linear regressions, both symmetrical and non-symmetrical, for Sérsic/core-Sérsic and for early/late-type galaxies. Symmetrical regressions are meant to be compared with theoretical expectations, whereas non-symmetrical direct ($M_{\rm BH}|X$) regressions – which minimize the scatter in the $\log(M_{\rm BH})$ direction – can be used to predict black hole masses.

4. RESULTS AND DISCUSSION

4.1. *Black hole mass – galaxy luminosity*

The $M_{\rm BH}-L_{\rm gal}$ diagram is shown in Figure 1. Four spiral galaxies had their total luminosities underestimated (see Section 2) and thus are not included in the linear regression analysis (see Table 2).

Läsker et al. (2014b) analyzed a sample of 35 galaxies, among which only four were classified as spiral galaxies, and claimed that the $M_{\rm BH}-L_{\rm sph}$ and $M_{\rm BH}-L_{\rm gal}$ relations, which they fit with a single power-law, have consistent intrinsic scatter. Here, instead, thanks to our galaxy sample that includes 17 spiral galaxies, we show that the claim made by Läsker et al. (2014b) is valid only for early-type galaxies. Our $M_{\rm BH}-L_{\rm sph}$ relation for 66 galaxies, irrespective of their morphological type, has an intrinsic scatter $\epsilon_{(Y|X)} = 0.51 \pm 0.06$ dex (forward linear regression) and $\epsilon_{(X|Y)} = 0.60 \pm 0.09$ dex (inverse linear regression), whereas our $M_{\rm BH}-L_{\rm gal}$ relation for 62 ($= 66-4$) galaxies has $\epsilon_{(Y|X)} = 0.63 \pm 0.07$ dex and $\epsilon_{(X|Y)} = 0.91 \pm 0.17$ dex. However, when considering only early-type galaxies, we find that the $M_{\rm BH}-L_{\rm sph}$ and $M_{\rm BH}-L_{\rm gal}$ relations have the same level of intrinsic scatter.

Because the value of the intrinsic scatter depends on the size of the uncertainties associated with the absolute magnitudes[7], we tested the robustness of our last conclusion by increasing the error associated with $L_{\rm gal}$ (we originally assumed 0.25 mag). The intrinsic scatter of the $M_{\rm BH}-L_{\rm gal}$ relation becomes smaller than that of the $M_{\rm BH}-L_{\rm sph}$ relation when assuming an error of $L_{\rm gal} \geq 0.7$ mag, which would be oddly larger than the typical error of $L_{\rm sph}$ used here and also significantly larger than the errors of $L_{\rm gal}$ commonly assumed in the literature. Hence, we conclude that our determination of the intrinsic scatter is reliable, and that $M_{\rm BH}$ correlates equally

[7] The smaller (larger) the uncertainties, the larger (smaller) the intrinsic scatter.

TABLE 1
Galaxy sample.

Galaxy	**Type**	**Core**	**Distance**	$M_{\mathbf{BH}}$	$MAG_{\mathbf{sph}}$	$MAG_{\mathbf{gal}}$	**[3.6] − [4.5]**	$M_{*,\mathbf{sph}}$
			[Mpc]	[10^8 $M_\odot$]	[mag]	[mag]	[mag]	[10^{10} $M_\odot$]
(1)	(2)	(3)	(4)	(5)	(6)	(7)	(8)	(9)
IC 1459	E	yes	28.4	24^{+10}_{-10}	$-26.15^{+0.18}_{-0.11}$	-26.15 ± 0.25	−0.12	27^{+30}_{-23}
IC 2560	Sp (bar)	no?	40.7	$0.044^{+0.044}_{-0.022}$	$-22.27^{+0.66}_{-0.58}$	-24.76 ± 0.25	−0.08	$1.0^{+1.8}_{-0.6}$
IC 4296	E	yes?	40.7	11^{+2}_{-2}	$-26.35^{+0.18}_{-0.11}$	-26.35 ± 0.25	−0.12	31^{+34}_{-26}
M104	S0/Sp	yes	9.5	$6.4^{+0.4}_{-0.4}$	$-23.91^{+0.66}_{-0.58}$	-25.21 ± 0.25	−0.12	$3.4^{+5.8}_{-1.9}$
M105	E	yes	10.3	4^{+1}_{-1}	$-24.29^{+0.66}_{-0.58}$	-24.29 ± 0.25	−0.10	$5.6^{+9.5}_{-3.0}$
M106	Sp (bar)	no	7.2	$0.39^{+0.01}_{-0.01}$	$-21.11^{+0.18}_{-0.11}$	-24.04 ± 0.25	−0.08	$0.37^{+0.41}_{-0.31}$
M31	Sp (bar)	no	0.7	$1.4^{+0.9}_{-0.3}$	$-22.74^{+0.18}_{-0.11}$	-24.67 ± 0.25	−0.09	$1.5^{+1.6}_{-1.3}$
M49	E	yes	17.1	25^{+3}_{-1}	$-26.54^{+0.18}_{-0.11}$	-26.54 ± 0.25	−0.12	39^{+43}_{-33}
M59	E	no	17.8	$3.9^{+0.4}_{-0.4}$	$-25.18^{+0.18}_{-0.11}$	-25.27 ± 0.25	−0.09	14^{+15}_{-11}
M64	Sp	no?	7.3	$0.016^{+0.004}_{-0.004}$	$-21.54^{+0.18}_{-0.11}$	-24.24 ± 0.25	−0.06	$0.64^{+0.71}_{-0.55}$
M81	Sp (bar)	no	3.8	$0.74^{+0.21}_{-0.11}$	$-23.01^{+0.88}_{-0.66}$	-24.43 ± 0.25	−0.09	$1.9^{+3.6}_{-0.9}$
M84	E	yes	17.9	$9.0^{+0.9}_{-0.8}$	$-26.01^{+0.66}_{-0.58}$	-26.01 ± 0.25	−0.10	28^{+47}_{-15}
M87	E	yes	15.6	$58.0^{+3.5}_{-3.5}$	$-26.00^{+0.66}_{-0.58}$	-26.00 ± 0.25	−0.11	26^{+44}_{-14}
M89	E	yes	14.9	$4.7^{+0.5}_{-0.5}$	$-24.48^{+0.66}_{-0.58}$	-24.74 ± 0.25	−0.11	$6.3^{+10.7}_{-3.4}$
M94	Sp (bar)	no?	4.4	$0.060^{+0.014}_{-0.014}$	$-22.08^{+0.18}_{-0.11}$	≤ -23.36	−0.07	$1.00^{+1.11}_{-0.85}$
M96	Sp (bar)	no	10.1	$0.073^{+0.015}_{-0.015}$	$-22.15^{+0.18}_{-0.11}$	-24.20 ± 0.25	−0.08	$0.97^{+1.08}_{-0.83}$
NGC 0524	S0	yes	23.3	$8.3^{+2.7}_{-1.3}$	$-23.19^{+0.18}_{-0.11}$	-24.92 ± 0.25	−0.09	$2.2^{+2.5}_{-1.9}$
NGC 0821	E	no	23.4	$0.39^{+0.26}_{-0.09}$	$-24.00^{+0.88}_{-0.66}$	-24.26 ± 0.25	−0.09	$4.7^{+8.7}_{-2.1}$
NGC 1023	S0 (bar)	no	11.1	$0.42^{+0.04}_{-0.04}$	$-22.82^{+0.18}_{-0.11}$	-24.20 ± 0.25	−0.10	$1.5^{+1.7}_{-1.3}$
NGC 1300	Sp (bar)	no	20.7	$0.73^{+0.69}_{-0.35}$	$-22.06^{+0.66}_{-0.58}$	-24.16 ± 0.25	−0.10	$0.70^{+1.19}_{-0.38}$
NGC 1316	merger	no	18.6	$1.50^{+0.75}_{-0.80}$	$-24.89^{+0.66}_{-0.58}$	-26.48 ± 0.25	−0.10	$9.5^{+16.2}_{-5.2}$
NGC 1332	E/S0	no	22.3	14^{+2}_{-2}	$-24.89^{+0.88}_{-0.66}$	-24.95 ± 0.25	−0.12	$8.2^{+15.0}_{-3.6}$
NGC 1374	E	no?	19.2	$5.8^{+0.5}_{-0.5}$	$-23.68^{+0.18}_{-0.11}$	-23.70 ± 0.25	−0.09	$3.6^{+4.0}_{-3.0}$
NGC 1399	E	yes	19.4	$4.7^{+0.6}_{-0.6}$	$-26.43^{+0.18}_{-0.11}$	-26.46 ± 0.25	−0.12	33^{+37}_{-28}
NGC 2273	Sp (bar)	no	28.5	$0.083^{+0.004}_{-0.004}$	$-23.00^{+0.66}_{-0.58}$	-24.21 ± 0.25	−0.08	$2.0^{+3.4}_{-1.1}$
NGC 2549	S0 (bar)	no	12.3	$0.14^{+0.02}_{-0.13}$	$-21.25^{+0.18}_{-0.11}$	-22.60 ± 0.25	−0.10	$0.35^{+0.39}_{-0.30}$
NGC 2778	S0 (bar)	no	22.3	$0.15^{+0.09}_{-0.10}$	$-20.80^{+0.66}_{-0.58}$	-22.44 ± 0.25	−0.09	$0.25^{+0.43}_{-0.14}$
NGC 2787	S0 (bar)	no	7.3	$0.40^{+0.04}_{-0.05}$	$-20.11^{+0.66}_{-0.58}$	-22.28 ± 0.25	−0.10	$0.12^{+0.20}_{-0.07}$
NGC 2974	Sp (bar)	no	20.9	$1.7^{+0.2}_{-0.2}$	$-22.95^{+0.66}_{-0.58}$	-24.16 ± 0.25	−0.09	$1.8^{+3.1}_{-1.0}$
NGC 3079	Sp (bar)	no?	20.7	$0.024^{+0.024}_{-0.012}$	$-23.01^{+0.66}_{-0.58}$	≤ -24.45	−0.07	$2.4^{+4.0}_{-1.3}$
NGC 3091	E	yes	51.2	36^{+1}_{-2}	$-26.28^{+0.18}_{-0.11}$	-26.28 ± 0.25	−0.12	30^{+34}_{-26}
NGC 3115	E/S0	no	9.4	$8.8^{+10.0}_{-2.7}$	$-24.22^{+0.18}_{-0.11}$	-24.40 ± 0.25	−0.11	$4.9^{+5.4}_{-4.1}$
NGC 3227	Sp (bar)	no	20.3	$0.14^{+0.10}_{-0.06}$	$-21.76^{+0.66}_{-0.58}$	-24.26 ± 0.25	−0.08	$0.67^{+1.15}_{-0.37}$
NGC 3245	S0 (bar)	no	20.3	$2.0^{+0.5}_{-0.5}$	$-22.43^{+0.18}_{-0.11}$	-23.88 ± 0.25	−0.10	$1.0^{+1.1}_{-0.9}$
NGC 3377	E	no	10.9	$0.77^{+0.04}_{-0.06}$	$-23.49^{+0.66}_{-0.58}$	-23.57 ± 0.25	−0.06	$4.0^{+6.8}_{-2.2}$
NGC 3384	S0 (bar)	no	11.3	$0.17^{+0.01}_{-0.02}$	$-22.43^{+0.18}_{-0.11}$	-23.74 ± 0.25	−0.08	$1.2^{+1.3}_{-1.0}$
NGC 3393	Sp (bar)	no	55.2	$0.34^{+0.02}_{-0.02}$	$-23.48^{+0.66}_{-0.58}$	-25.29 ± 0.25	−0.10	$2.8^{+4.7}_{-1.5}$
NGC 3414	E	no	24.5	$2.4^{+0.3}_{-0.3}$	$-24.35^{+0.18}_{-0.11}$	-24.42 ± 0.25	−0.09	$6.5^{+7.2}_{-5.5}$
NGC 3489	S0/Sp (bar)	no	11.7	$0.058^{+0.008}_{-0.008}$	$-21.13^{+0.66}_{-0.58}$	-23.07 ± 0.25	−0.06	$0.42^{+0.72}_{-0.23}$
NGC 3585	E	no	19.5	$3.1^{+1.4}_{-0.6}$	$-25.52^{+0.66}_{-0.58}$	-25.55 ± 0.25	−0.10	18^{+30}_{-10}
NGC 3607	E	no	22.2	$1.3^{+0.5}_{-0.5}$	$-25.36^{+0.66}_{-0.58}$	-25.45 ± 0.25	−0.10	15^{+25}_{-8}
NGC 3608	E	yes	22.3	$2.0^{+1.1}_{-0.6}$	$-24.50^{+0.66}_{-0.58}$	-24.50 ± 0.25	−0.08	$7.8^{+13.4}_{-4.3}$
NGC 3842	E	yes	98.4	97^{+30}_{-26}	$-27.00^{+0.18}_{-0.11}$	-27.04 ± 0.25	−0.11	61^{+68}_{-52}
NGC 3998	S0 (bar)	no	13.7	$8.1^{+2.0}_{-1.9}$	$-22.32^{+0.88}_{-0.66}$	-23.53 ± 0.25	−0.12	$0.78^{+1.43}_{-0.35}$
NGC 4026	S0 (bar)	no	13.2	$1.8^{+0.6}_{-0.3}$	$-21.58^{+0.88}_{-0.66}$	-23.16 ± 0.25	−0.09	$0.50^{+0.92}_{-0.22}$
NGC 4151	Sp (bar)	no	20.0	$0.65^{+0.07}_{-0.07}$	$-23.40^{+0.66}_{-0.58}$	-24.44 ± 0.25	−0.09	$2.8^{+4.8}_{-1.5}$
NGC 4261	E	yes	30.8	5^{+1}_{-1}	$-25.72^{+0.66}_{-0.58}$	-25.76 ± 0.25	−0.12	18^{+30}_{-10}
NGC 4291	E	yes	25.5	$3.3^{+0.9}_{-2.5}$	$-24.05^{+0.66}_{-0.58}$	-24.05 ± 0.25	−0.11	$3.9^{+6.7}_{-2.1}$
NGC 4388	Sp (bar)	no?	17.0	$0.075^{+0.002}_{-0.002}$	$-21.26^{+0.88}_{-0.66}$	≤ -23.50	−0.07	$0.46^{+0.85}_{-0.21}$
NGC 4459	S0	no	15.7	$0.68^{+0.13}_{-0.13}$	$-23.48^{+0.66}_{-0.58}$	-24.01 ± 0.25	−0.09	$2.9^{+5.0}_{-1.6}$
NGC 4473	E	no	15.3	$1.2^{+0.4}_{-0.9}$	$-23.88^{+0.66}_{-0.58}$	-24.11 ± 0.25	−0.10	$3.9^{+6.6}_{-2.1}$
NGC 4564	S0	no	14.6	$0.60^{+0.03}_{-0.09}$	$-22.30^{+0.18}_{-0.11}$	-22.99 ± 0.25	−0.11	$0.82^{+0.91}_{-0.70}$
NGC 4596	S0 (bar)	no	17.0	$0.79^{+0.38}_{-0.33}$	$-22.73^{+0.18}_{-0.11}$	-24.18 ± 0.25	−0.08	$1.6^{+1.7}_{-1.3}$

Galaxy	**Type**	**Core**	**Distance**	$M_{\rm BH}$	$MAG_{\rm sph}$	$MAG_{\rm gal}$	**[3.6] − [4.5]**	$M_{*,\rm sph}$
			[Mpc]	[10^8 M$_\odot$]	[mag]	[mag]	[mag]	[10^{10} M$_\odot$]
(1)	(2)	(3)	(4)	(5)	(6)	(7)	(8)	(9)
NGC 4697	E	no	11.4	$1.8^{+0.2}_{-0.1}$	$-24.82^{+0.88}_{-0.66}$	-24.94 ± 0.25	-0.09	10^{+18}_{-4}
NGC 4889	E	yes	103.2	210^{+160}_{-160}	$-27.54^{+0.18}_{-0.11}$	-27.54 ± 0.25	-0.12	91^{+101}_{-77}
NGC 4945	Sp (bar)	no?	3.8	$0.014^{+0.014}_{-0.007}$	$-20.96^{+0.66}_{-0.58}$	≤ -23.79	-0.06	$0.36^{+0.62}_{-0.20}$
NGC 5077	E	yes	41.2	$7.4^{+4.7}_{-3.0}$	$-25.45^{+0.18}_{-0.11}$	-25.45 ± 0.25	-0.11	15^{+17}_{-13}
NGC 5128	merger	no?	3.8	$0.45^{+0.17}_{-0.10}$	$-23.89^{+0.88}_{-0.66}$	-24.97 ± 0.25	-0.07	$5.0^{+9.1}_{-2.2}$
NGC 5576	E	no	24.8	$1.6^{+0.3}_{-0.4}$	$-24.44^{+0.18}_{-0.11}$	-24.44 ± 0.25	-0.09	$7.1^{+7.9}_{-6.0}$
NGC 5845	S0	no	25.2	$2.6^{+0.4}_{-1.5}$	$-22.96^{+0.88}_{-0.66}$	-23.10 ± 0.25	-0.12	$1.4^{+2.6}_{-0.6}$
NGC 5846	E	yes	24.2	11^{+1}_{-1}	$-25.81^{+0.66}_{-0.58}$	-25.81 ± 0.25	-0.10	22^{+38}_{-12}
NGC 6251	E	yes?	104.6	5^{+2}_{-2}	$-26.75^{+0.18}_{-0.11}$	-26.75 ± 0.25	-0.12	46^{+51}_{-39}
NGC 7052	E	yes	66.4	$3.7^{+2.6}_{-1.5}$	$-26.32^{+0.18}_{-0.11}$	-26.32 ± 0.25	-0.11	33^{+36}_{-28}
NGC 7619	E	yes	51.5	25^{+8}_{-3}	$-26.35^{+0.66}_{-0.58}$	-26.41 ± 0.25	-0.11	33^{+56}_{-18}
NGC 7768	E	yes	112.8	13^{+5}_{-4}	$-26.90^{+0.66}_{-0.58}$	-26.90 ± 0.25	-0.11	57^{+98}_{-31}
UGC 03789	Sp (bar)	no?	48.4	$0.108^{+0.005}_{-0.005}$	$-22.77^{+0.88}_{-0.66}$	-24.20 ± 0.25	-0.07	$1.9^{+3.4}_{-0.8}$

NOTE. — *Column (1)*: Galaxy name. *Column (2)*: Morphological type (E=elliptical, S0=lenticular, Sp=spiral, merger). The morphological classification of four galaxies is uncertain (E/S0 or S0/Sp). The presence of a bar is indicated. *Column (3)*: Presence of a partially depleted core. The question mark is used when the classification has come from the velocity dispersion criteria mentioned in Section 2. *Column (4)*: Distance. *Column (5)*: Black hole mass. *Column (6)*: Absolute 3.6 μm bulge magnitude. Bulge magnitudes come from our state-of-the-art multicomponent galaxy decompositions (*Paper I*), which include bulges, disks, bars, spiral arms, rings, haloes, extended or unresolved nuclear sources and partially depleted cores, and that – for the first time – were checked to be consistent with the galaxy kinematics. The uncertainties were estimated with a method that takes into account systematic errors, which are typically not considered by popular 2D fitting codes. *Column (7)*: Absolute 3.6 μm galaxy magnitude. Four galaxies had their magnitudes overestimated, which are given here as upper limits. *Column (8)*: [3.6] − [4.5] colour. *Column (9)*: Bulge stellar mass.

well with $L_{\rm sph}$ and $L_{\rm gal}$ only for early-type galaxies, but not for all (early+late) galaxies.

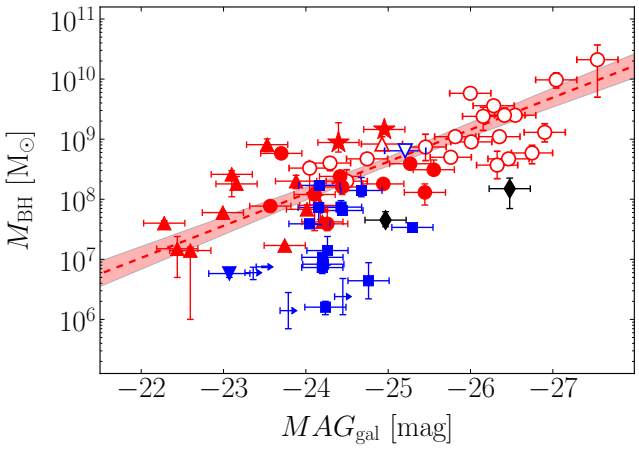

FIG. 1.— Black hole mass plotted against 3.6 μm galaxy absolute magnitude. Symbols are coded according to the galaxy morphological type: red circle = E, red star = E/S0, red upward triangle = S0, blue downward triangle = S0/Sp, blue square = Sp, black diamond = merger. Empty symbols represent core-Sérsic spheroids, whereas filled symbols are used for Sérsic spheroids. Four spiral galaxies had their magnitudes overestimated and are shown as upper limits. The red dashed line indicates the BCES bisector linear regression for the 45 early-type galaxies (E+S0), with the red shaded area denoting its 1σ uncertainty. We were not able to obtain any meaningful linear regression for the 13 (= 17−4) late-type (Sp) galaxies. $M_{\rm BH}$ correlates equally well with $L_{\rm sph}$ and $L_{\rm gal}$ only for early-type galaxies, but not for all (early+late) galaxies.

4.2. *Black hole mass – spheroid luminosity*

The $M_{\rm BH}-L_{\rm sph}$ diagram is shown in Figure 2, and the linear regression analysis is presented in Table 3.
Sérsic and core-Sérsic spheroids have slopes consistent with each other (within their 1σ uncertainties), in disagreement with the findings of GS13. The slope that we obtained for core-Sérsic spheroids ($M_{\rm BH}\propto L_{\rm sph}^{1.18\pm0.20}$) is consistent with the slope reported by GS13 in the K_s-band for the same population ($M_{\rm BH}\propto L_{\rm sph}^{1.10\pm0.20}$). However, the slope that we determined for Sérsic spheroids ($M_{\rm BH}\propto L_{\rm sph}^{1.53\pm0.20}$) is notably shallower than that found by GS13 ($M_{\rm BH}\propto L_{\rm sph}^{2.73\pm0.55}$). Although the Sérsic/core-Sérsic classification used by GS13 slightly differs[8] from the classification used here, the main cause of such inconsistency is that the bulge-to-total ratios obtained from our galaxy decompositions are different from those assumed by GS13 to convert galaxy luminosities into bulge luminosities. Our bulge-to-total ratios for low-luminosity Sérsic spheroids (3.6 μm $MAG_{\rm sph}\gtrsim -22$ mag) are smaller than those used by GS13. The host galaxies of such bulges are late-type, spiral galaxies, which typically present a complex morphology (bars, double bars, embedded disks, nuclear components, etc). Our sophisticated galaxy models account for the extra components, while the bulge-to-total ratios of GS13 were based on simple literature Sérsic-bulge/exponential-disk decompositions which overestimated the bulge luminosity. This results in our bulge magnitudes being on average ∼1 mag fainter than in GS13, after accounting for the different wavelength of the data. At the same time, our bulge-to-total ratios for the high-luminosity Sérsic spheroids (3.6 μm $MAG_{\rm sph}\lesssim -24$ mag) are on average larger than those adopted by GS13. In this regime, the host systems are early-type galaxies that feature intermediate-scale disks[9]. Past bulge/disk decompositions failed to correctly identify the extent of such disks and treated them as large-scale disks, thus underestimating the bulge luminosity. The magnitudes that we obtained for such spheroids are on average ∼1 mag brighter than in GS13. These two effects explain the shallower slope that we obtained for the Sérsic spheroids.
We have seen that the change in slope of the $M_{\rm BH}-L_{\rm sph}$ relation – which is expected for consistency with other scaling relations (a single power-law $M_{\rm BH}-\sigma$ correlation and a double power-law $L_{\rm sph}-\sigma$ correlation) – cannot be attributed to the division between the two populations of Sérsic and core-Sérsic spheroids. We now test a new hypothesis, where the change in slope is ascribed to the different formation mechanisms of early- and late-type galaxies. If this hypothesis is correct, the spheroids of early-type galaxies will follow $M_{\rm BH}\propto L_{\rm sph}^{\sim1}$, whereas the spheroids of late-type galaxies will have $M_{\rm BH}\propto L_{\rm sph}^{\sim2.5}$. First, we checked that elliptical and lenticular galaxies, taken separately, have slopes consistent with each other, and thus, taken together, they define a single *red sequence* in the $M_{\rm BH}-L_{\rm sph}$ diagram. We then fit the bulges of early- and late-type galaxies with two separate log-linear regressions, and obtained $M_{\rm BH}\propto L_{\rm sph}^{1.00\pm0.10}$ and $M_{\rm BH}\propto L_{\rm sph}^{2.88\pm0.68}$ respectively, in excellent agreement with the theoretical expectations of our hypothesis. We point out the unsuitability of Pearson's and Spearman's correlation coefficients because they do not take into account the error bars on our data. Similarly, a visual inspection of the plotted data requires us to take into account the error bars when judging-by-eye the strength of a correlation. We have therefore relied on the quantitative regression analysis rather than subjective approaches.

4.2.1. *Pseudo- versus classical bulges*

Current views distinguish between classical bulges, which are considered to be spheroidal, pressure-supported systems, formed through violent processes, such as hierarchical clustering via minor mergers, and pseudo-bulges, thought to be disk-like, rotation-supported systems, built from secular evolution processes, such as instabilities of their surrounding disk or bar. Pseudo-bulges are notoriously hard to identify (Graham 2013, 2014, 2015a,c). For example, mergers can create bulges that rotate (e.g. Bekki 2010; Keselman & Nusser 2012), and bars can spin-up classical bulges

[8] The classification has changed for the galaxies NGC 1316, NGC 1332 and NGC 3998.

[9] Intermediate-scale disks are disks of stars fully embedded in the spheroidal component of their galaxy. They are typical of "disky" elliptical galaxies (e.g. NGC 3377), but they can also be found in other types of host galaxies. They can be considered an intermediate class between nuclear disks, with sizes ∼10 − 100 pc, and large-scale disks, that encase the bulge and dominate the light at large radii.

TABLE 2
LINEAR REGRESSION ANALYSIS OF THE $M_{\rm BH} - L_{\rm gal}$ DIAGRAM.

Subsample (size)	Regression	α	β	$\langle MAG_{\rm gal}\rangle$	ϵ	Δ
	$\log[M_{\rm BH}/{\rm M}_\odot] = \alpha + \beta[(MAG_{\rm gal} - \langle MAG_{\rm gal}\rangle)/{\rm mag}]$					
All (62)	BCES $(Y\|X)$	8.26 ± 0.08	-0.49 ± 0.06	-24.78	–	0.64
	BCES $(X\|Y)$	8.26 ± 0.12	-1.01 ± 0.15	-24.78	–	0.92
	BCES Bisector	8.26 ± 0.09	-0.72 ± 0.07	-24.78	–	0.71
	mFITEXY $(Y\|X)$	$8.26^{+0.08}_{-0.08}$	$-0.49^{+0.06}_{-0.07}$	-24.78	$0.61^{+0.07}_{-0.06}$	0.64
	mFITEXY $(X\|Y)$	$8.26^{+0.11}_{-0.12}$	$-1.03^{+0.13}_{-0.16}$	-24.78	$0.88^{+0.10}_{-0.08}$	0.93
	mFITEXY Bisector	$8.26^{+0.10}_{-0.10}$	$-0.73^{+0.09}_{-0.10}$	-24.78	–	0.71
	`linmix_err` $(Y\|X)$	8.26 ± 0.09	-0.49 ± 0.07	-24.78	0.63 ± 0.07	0.64
	`linmix_err` $(X\|Y)$	8.26 ± 0.12	-1.02 ± 0.15	-24.78	0.91 ± 0.17	0.93
	`linmix_err` Bisector	8.26 ± 0.10	-0.72 ± 0.15	-24.78	–	0.71
Early-type (E+S0) (45)	BCES $(Y\|X)$	8.56 ± 0.07	-0.44 ± 0.05	-24.88	–	0.45
	BCES $(X\|Y)$	8.56 ± 0.08	-0.64 ± 0.05	-24.88	–	0.53
	BCES Bisector	8.56 ± 0.07	-0.53 ± 0.04	-24.88	–	0.47
	mFITEXY $(Y\|X)$	$8.56^{+0.06}_{-0.06}$	$-0.42^{+0.05}_{-0.05}$	-24.88	$0.41^{+0.06}_{-0.05}$	0.45
	mFITEXY $(X\|Y)$	$8.56^{+0.08}_{-0.08}$	$-0.66^{+0.07}_{-0.08}$	-24.88	$0.51^{+0.07}_{-0.06}$	0.55
	mFITEXY Bisector	$8.56^{+0.07}_{-0.07}$	$-0.54^{+0.06}_{-0.06}$	-24.88	–	0.47
	`linmix_err` $(Y\|X)$	8.56 ± 0.07	-0.42 ± 0.06	-24.88	0.43 ± 0.06	0.45
	`linmix_err` $(X\|Y)$	8.56 ± 0.09	-0.65 ± 0.08	-24.88	0.53 ± 0.10	0.54
	`linmix_err` Bisector	8.56 ± 0.08	-0.53 ± 0.10	-24.88	–	0.47

NOTE. — For each subsample, we indicate $\langle MAG_{\rm gal}\rangle$, its average value of galaxy magnitudes. In the last two columns, we report ϵ, the intrinsic scatter, and Δ, the total rms scatter in the $\log(M_{\rm BH})$ direction. Four spiral galaxies had their luminosities underestimated and thus are not included in the linear regression analysis (the sample of all galaxies contains 66-4=62 objects). When considering all galaxies, irrespective of their morphological type, the $M_{\rm BH} - L_{\rm gal}$ correlation is weaker than the $M_{\rm BH} - L_{\rm sph}$ correlation, in terms of intrinsic scatter. However, when considering only early-type galaxies, the $M_{\rm BH} - L_{\rm gal}$ and $M_{\rm BH} - L_{\rm sph}$ correlations have consistent intrinsic scatter.

(e.g. Saha et al. 2012), thus rotation is not a definitive signature of a pseudo-bulge. Furthermore, many galaxies host both a pseudo- and a classical bulge (e.g. Erwin et al. 2003, 2015; Athanassoula 2005; Gadotti 2009; MacArthur et al. 2009; dos Anjos & da Silva 2013; Seidel et al. 2015). In the recent literature, pseudo- and classical bulges have frequently been divided at the Sérsic index $n_{\rm sph} = 2$ (e.g. Sani et al. 2011; Beifiori et al. 2012), although, from a selection of hundreds of disc galaxies imaged in the K-band, Graham & Worley (2008) observed no bimodality in the bulge Sérsic indices about $n_{\rm sph} = 2$ or any other value. While pseudo-bulges are expected to have exponential-like surface brightness profiles ($n_{\rm sph} \simeq 1$), being disky components that formed from their surrounding exponential disks (e.g. Bardeen 1975; Hohl 1975; Combes & Sanders 1981; Combes et al. 1990; Pfenniger & Friedli 1991), it has been shown that mergers can create bulges with $n_{\rm sph} < 2$ (e.g. Eliche-Moral et al. 2011; Scannapieco et al. 2011; Querejeta et al. 2015), just as low-luminosity elliptical galaxies (not built from the secular evolution of a disk) are well known to have $n_{\rm sph} < 2$ and even $n_{\rm sph} < 1$ (e.g. Davies et al. 1988; Young & Currie 1994; Jerjen et al. 2000). The use of the Sérsic index to identify pseudo-bulges is thus a dangerous practice.

Sani et al. (2011) reported that pseudo-bulges – which they labelled as such according to the $n_{\rm sph} < 2$ criterion – with low black hole masses ($M_{\rm BH} < 10^7$ M$_\odot$) are significantly displaced from the correlation traced by their (classical) bulges with $n_{\rm sph} > 2$. In Figure 3, we show the distribution of spheroid Sérsic indices[10] in the $M_{\rm BH} - L_{\rm sph}$ diagram. Our aim is to check whether bulges with $n_{\rm sph} < 2$ are offset to lower black hole masses from the correlation defined by bulges with $n_{\rm sph} > 2$. To do this, we fit a symmetrical linear regression to the bulges that have $n_{\rm sph} > 2$ and we compute the vertical offset of all bulges from the regression. In Figure 3, we plot the vertical offset against $n_{\rm sph}$. Among the 23 bulges with $n_{\rm sph} < 2$, 12 have a positive vertical offset and 11 have a negative vertical offset. Kormendy (2015) provides a list of many pseudo-bulges classification criteria, including the divide at $n_{\rm sph} = 2$, and cautions that each individual criterion has a failure rate of 0-25%. If this is true, we should have that no less than 75% of bulges with $n_{\rm sph} < 2$ display a negative vertical offset[11]. What we observe, instead, is that there are the same number of bulges with $n_{\rm sph} < 2$ lying above and below the correlation defined by bulges with $n_{\rm sph} > 2$, and that the amplitude of their offset is the same ($\lesssim 1.5$ dex). That is, bulges with $n_{\rm sph} < 2$ do not appear to be offset from the correlation traced by bulges with $n_{\rm sph} > 2$.

4.3. *Black hole mass – spheroid stellar mass*

Finally, we present the $M_{\rm BH} - M_{*,\rm sph}$ diagram in Figure 5, and its linear regression analysis in Table 4. The bulges of early-type galaxies follow $M_{\rm BH} \propto M_{*,\rm sph}^{1.04\pm0.10}$, consistent with a dry-merging formation scenario, and define a tight *red sequence* with intrinsic scatter $\epsilon_{(Y|X)} = 0.43 \pm 0.06$ dex. On the other hand, the bulges of spiral galaxies trace a steeper *blue sequence*, whose slope is less well constrained due to the small size of the subsample and, more importantly, to the small range in $M_{*,\rm sph}$ that

[10] The spheroid Sérsic indices are taken from our galaxy decompositions (*Paper I*).

[11] One reaches the same conclusion when using the vertical offset from the correlation defined by bulges with $n_{\rm sph} > 3$ or even $n_{\rm sph} > 4$. There are 13 and 10 bulges with $n_{\rm sph} < 2$ that lie above and below, respectively, the correlation traced by bulges with $n_{\rm sph} > 3$. Similarly, there are 15 and 8 bulges with $n_{\rm sph} < 2$ that lie above and below, respectively, the correlation traced by bulges with $n_{\rm sph} > 4$.

TABLE 3
LINEAR REGRESSION ANALYSIS OF THE $M_{\rm BH} - L_{\rm sph}$ DIAGRAM.

Subsample (size)	**Regression**	$\boldsymbol{\alpha}$	$\boldsymbol{\beta}$	$\langle MAG_{\rm sph}\rangle$	$\boldsymbol{\epsilon}$	$\boldsymbol{\Delta}$
	$\log[M_{\rm BH}/{\rm M}_\odot] = \alpha + \beta[(MAG_{\rm sph} - \langle MAG_{\rm sph}\rangle)/{\rm mag}]$					
All (66)	BCES $(Y\|X)$	8.16 ± 0.07	-0.44 ± 0.04	-23.86	–	0.56
	BCES $(X\|Y)$	8.16 ± 0.08	-0.61 ± 0.05	-23.86	–	0.68
	BCES Bisector	8.16 ± 0.07	-0.52 ± 0.04	-23.86	–	0.60
	mFITEXY $(Y\|X)$	$8.17^{+0.06}_{-0.07}$	$-0.43^{+0.03}_{-0.04}$	-23.86	$0.49^{+0.06}_{-0.05}$	0.56
	mFITEXY $(X\|Y)$	$8.15^{+0.07}_{-0.08}$	$-0.61^{+0.05}_{-0.05}$	-23.86	$0.58^{+0.07}_{-0.06}$	0.68
	mFITEXY Bisector	$8.16^{+0.07}_{-0.07}$	$-0.51^{+0.04}_{-0.04}$	-23.86	–	0.60
	`linmix_err` $(Y\|X)$	8.16 ± 0.07	-0.42 ± 0.04	-23.86	0.51 ± 0.06	0.56
	`linmix_err` $(X\|Y)$	8.16 ± 0.09	-0.60 ± 0.06	-23.86	0.60 ± 0.09	0.67
	`linmix_err` Bisector	8.16 ± 0.08	-0.51 ± 0.09	-23.86	–	0.59
$n > 2$ (43)	BCES $(Y\|X)$	8.58 ± 0.07	-0.42 ± 0.06	-24.77	–	0.46
	BCES $(X\|Y)$	8.58 ± 0.08	-0.58 ± 0.06	-24.77	–	0.56
	BCES Bisector	8.58 ± 0.07	-0.50 ± 0.05	-24.77	–	0.49
	mFITEXY $(Y\|X)$	$8.57^{+0.07}_{-0.06}$	$-0.41^{+0.04}_{-0.04}$	-24.77	$0.38^{+0.06}_{-0.06}$	0.46
	mFITEXY $(X\|Y)$	$8.56^{+0.08}_{-0.08}$	$-0.57^{+0.06}_{-0.07}$	-24.77	$0.44^{+0.08}_{-0.11}$	0.55
	mFITEXY Bisector	$8.57^{+0.07}_{-0.07}$	$-0.49^{+0.05}_{-0.05}$	-24.77	–	0.49
	`linmix_err` $(Y\|X)$	8.56 ± 0.07	-0.39 ± 0.05	-24.77	0.40 ± 0.06	0.46
	`linmix_err` $(X\|Y)$	8.55 ± 0.09	-0.57 ± 0.08	-24.77	0.49 ± 0.10	0.55
	`linmix_err` Bisector	8.56 ± 0.08	-0.48 ± 0.10	-24.77	–	0.49
Core-Sérsic (22)	BCES $(Y\|X)$	9.06 ± 0.09	-0.32 ± 0.11	-25.73	–	0.42
	BCES $(X\|Y)$	9.06 ± 0.12	-0.65 ± 0.12	-25.73	–	0.61
	BCES Bisector	9.06 ± 0.10	-0.47 ± 0.08	-25.73	–	0.48
	mFITEXY $(Y\|X)$	$9.06^{+0.08}_{-0.09}$	$-0.26^{+0.08}_{-0.07}$	-25.73	$0.36^{+0.09}_{-0.06}$	0.42
	mFITEXY $(X\|Y)$	$9.03^{+0.15}_{-0.16}$	$-0.72^{+0.17}_{-0.31}$	-25.73	$0.61^{+0.14}_{-0.09}$	0.68
	mFITEXY Bisector	$9.05^{+0.12}_{-0.13}$	$-0.47^{+0.12}_{-0.17}$	-25.73	–	0.48
	`linmix_err` $(Y\|X)$	9.04 ± 0.10	-0.24 ± 0.09	-25.73	0.40 ± 0.08	0.42
	`linmix_err` $(X\|Y)$	9.03 ± 0.17	-0.69 ± 0.27	-25.73	0.68 ± 0.30	0.64
	`linmix_err` Bisector	9.04 ± 0.14	-0.44 ± 0.16	-25.73	–	0.46
Sérsic (44)	BCES $(Y\|X)$	7.71 ± 0.09	-0.41 ± 0.08	-22.92	–	0.61
	BCES $(X\|Y)$	7.71 ± 0.14	-0.86 ± 0.16	-22.92	–	0.93
	BCES Bisector	7.71 ± 0.10	-0.61 ± 0.08	-22.92	–	0.71
	mFITEXY $(Y\|X)$	$7.72^{+0.08}_{-0.09}$	$-0.41^{+0.07}_{-0.08}$	-22.92	$0.54^{+0.08}_{-0.07}$	0.61
	mFITEXY $(X\|Y)$	$7.72^{+0.14}_{-0.13}$	$-0.86^{+0.13}_{-0.19}$	-22.92	$0.77^{+0.13}_{-0.10}$	0.93
	mFITEXY Bisector	$7.72^{+0.11}_{-0.11}$	$-0.61^{+0.10}_{-0.12}$	-22.92	–	0.71
	`linmix_err` $(Y\|X)$	7.73 ± 0.09	-0.41 ± 0.08	-22.92	0.55 ± 0.08	0.61
	`linmix_err` $(X\|Y)$	7.73 ± 0.14	-0.86 ± 0.17	-22.92	0.79 ± 0.20	0.93
	`linmix_err` Bisector	7.73 ± 0.12	-0.62 ± 0.15	-22.92	–	0.71
Early-type (E+S0) (45)	BCES $(Y\|X)$	8.56 ± 0.07	-0.33 ± 0.04	-24.47	–	0.46
	BCES $(X\|Y)$	8.56 ± 0.08	-0.48 ± 0.05	-24.47	–	0.55
	BCES Bisector	$\mathbf{8.56 \pm 0.07}$	$\mathbf{-0.40 \pm 0.04}$	$\mathbf{-24.47}$	–	**0.49**
	mFITEXY $(Y\|X)$	$8.56^{+0.06}_{-0.06}$	$-0.32^{+0.03}_{-0.04}$	-24.47	$0.40^{+0.06}_{-0.05}$	0.46
	mFITEXY $(X\|Y)$	$8.54^{+0.08}_{-0.08}$	$-0.49^{+0.05}_{-0.06}$	-24.47	$0.49^{+0.08}_{-0.06}$	0.57
	mFITEXY Bisector	$8.55^{+0.07}_{-0.07}$	$-0.41^{+0.04}_{-0.05}$	-24.47	–	0.49
	`linmix_err` $(Y\|X)$	8.55 ± 0.07	-0.32 ± 0.04	-24.47	0.41 ± 0.06	0.46
	`linmix_err` $(X\|Y)$	8.55 ± 0.09	-0.48 ± 0.06	-24.47	0.51 ± 0.10	0.56
	`linmix_err` Bisector	8.55 ± 0.08	-0.40 ± 0.09	-24.47	–	0.49
Late-type (Sp) (17)	BCES $(Y\|X)$	7.18 ± 0.16	-0.79 ± 0.43	-22.33	–	0.70
	BCES $(X\|Y)$	7.18 ± 0.29	-1.71 ± 0.71	-22.33	–	1.26
	BCES Bisector	$\mathbf{7.18 \pm 0.20}$	$\mathbf{-1.15 \pm 0.27}$	$\mathbf{-22.33}$	–	**0.88**
	mFITEXY $(Y\|X)$	$7.20^{+0.15}_{-0.15}$	$-0.53^{+0.22}_{-0.24}$	-22.33	$0.55^{+0.15}_{-0.10}$	0.63
	mFITEXY $(X\|Y)$	$7.38^{+0.54}_{-0.36}$	$-2.02^{+0.71}_{-2.13}$	-22.33	$1.09^{+0.41}_{-0.24}$	1.50
	mFITEXY Bisector	$7.26^{+0.40}_{-0.28}$	$-1.03^{+0.33}_{-0.52}$	-22.33	–	0.82
	`linmix_err` $(Y\|X)$	7.24 ± 0.19	-0.46 ± 0.32	-22.33	0.63 ± 0.16	0.62
	`linmix_err` $(X\|Y)$	7.34 ± 0.43	-1.93 ± 1.30	-22.33	1.31 ± 0.97	1.43
	`linmix_err` Bisector	7.27 ± 0.33	-0.96 ± 0.50	-22.33	–	0.78

NOTE. — For each subsample, we indicate $\langle MAG_{\rm sph}\rangle$, its average value of spheroid magnitudes. In the last two columns, we report ϵ, the intrinsic scatter, and Δ, the total rms scatter in the $\log(M_{\rm BH})$ direction. Both the early- and late-type subsamples do not contain the two galaxies classified as S0/Sp and the two galaxies classified as mergers (45+17=66-2-2).

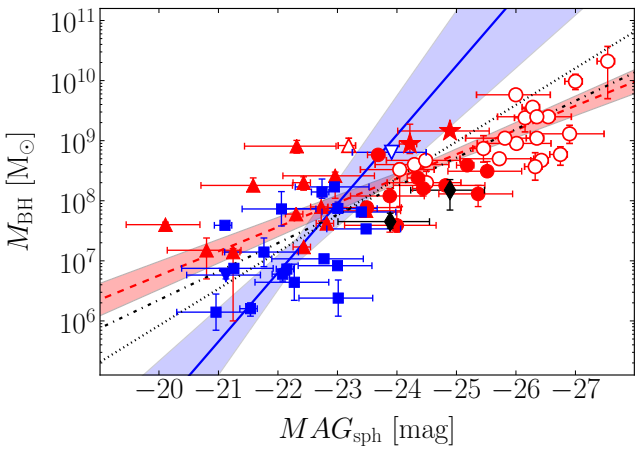

FIG. 2.— Black hole mass plotted against 3.6 μm spheroid absolute magnitude. Symbols are coded according to the galaxy morphological type: red circle = E, red star = E/S0, red upward triangle = S0, blue downward triangle = S0/Sp, blue square = Sp, black diamond = merger. Empty symbols represent core-Sérsic spheroids, whereas filled symbols are used for Sérsic spheroids. The red dashed line indicates the BCES bisector linear regression for the bulges of the 45 early-type (E+S0) galaxies, with the red shaded area denoting its 1σ uncertainty. The blue solid line shows the BCES bisector linear regression for the bulges of the 17 late-type (Sp) galaxies, with the blue shaded area denoting its 1σ uncertainty. The black dashed-dotted and dotted lines represent the BCES bisector linear regressions for the core-Sérsic and Sérsic spheroids, respectively.

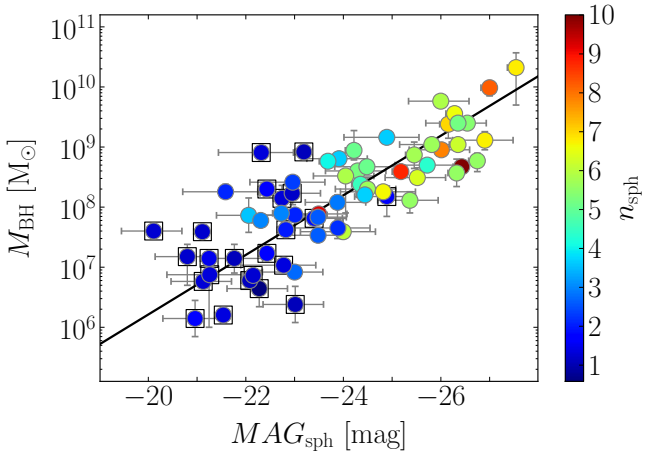

FIG. 3.— Black hole mass plotted against 3.6 μm spheroid absolute magnitude. Symbols are color coded according to the spheroid Sérsic index $n_{\rm sph}$. Bulges with $n_{\rm sph} < 2$, claimed by some to be pseudo-bulges, are marked with a square. The black solid line shows the BCES bisector linear regression for the spheroids that have $n_{\rm sph} \geq 2$, such that $M_{\rm BH} \propto L_{\rm sph}^{1.25\pm0.13}$.

the subsample spans. More data would be welcome to better constrain the slope of this *blue sequence*. For the bulges of spiral galaxies, the BCES code returns a log-linear relation with slope $= 3.00 \pm 1.30$, while the modified FITEXY routine finds a shallower (but still consistent within the 1σ uncertainty) slope $= 2.28^{+1.67}_{-1.01}$. The Bayesian estimator of Kelly (2007) fails in performing an inverse $(X|Y)$ linear regression for the subsample of

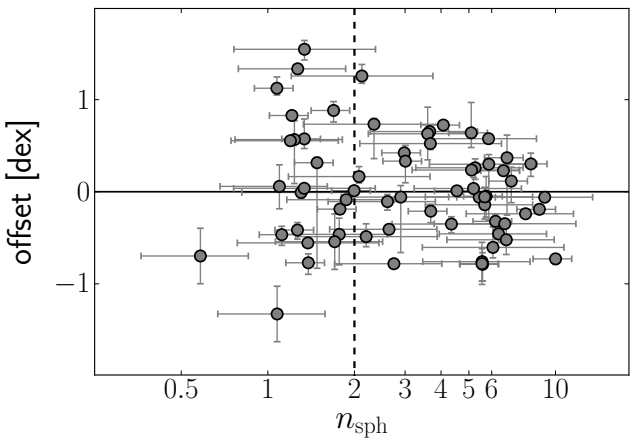

FIG. 4.— Vertical offset from the $M_{\rm BH} - L_{\rm sph}$ correlation defined by spheroids with $n_{\rm sph} \geq 2$ (see Figure 3), plotted against $n_{\rm sph}$. The vertical dashed line corresponds to $n_{\rm sph} = 2$. The horizontal solid line is equivalent to a zero vertical offset. Among the bulges with $n_{\rm sph} < 2$, 12 have a positive vertical offset and 11 have a negative vertical offset. Hence, bulges with $n_{\rm sph} < 2$ are not randomly offset to lower black hole masses from the correlation traced by bulges with $n_{\rm sph} \geq 2$.

spiral galaxies.

Using data from Jiang et al. (2011), Graham & Scott (2015) collected a sample of ∼140 low-redshift ($z \leq 0.35$, with a median redshift $\langle z \rangle = 0.085$) bulges hosting Active Galactic Nuclei (AGNs) with black hole masses $10^5 \lesssim M_{\rm BH}/{\rm M}_\odot \lesssim 2 \times 10^6$, and showed that they roughly follow the quadratic $M_{\rm BH} - M_{*,\rm sph}$ relation defined by Sérsic bulges. We anticipate here that the correlation traced by our bulges of spiral galaxies may track the location of the AGNs in the $M_{\rm BH} - M_{*,\rm sph}$ diagram. That is, the AGNs appear to be the low-mass continuation of the tentative *blue sequence* shown in Figure 5. We additionally note that the majority of our spiral galaxies host an AGN[12]. This topic will be investigated in Graham et al. (2015, *in preparation*) with a dedicated analysis.

5. CONCLUSIONS

GS warmly thanks Luca Cortese, Elisabete Lima Da Cunha and Gonzalo Diaz for useful discussion.
This research was supported by Australian Research Council funding through grants DP110103509 and FT110100263. This work is based on observations made with the IRAC instrument (Fazio et al. 2004) on-board the Spitzer Space Telescope, which is operated by the Jet Propulsion Laboratory, California Institute of Technology under a contract with NASA. This research has made use of the GOLDMine database (Gavazzi et al. 2003) and the NASA/IPAC Extragalactic Database (NED) which is operated by the Jet Propulsion Laboratory, California Institute of Technology, under contract with the National Aeronautics and Space Administra-

[12] According to the nuclear classification reported on NED (Nasa Extragalactic Database), among our 17 spiral galaxies, at least 12 host a Seyfert AGN and one hosts a LINER AGN.

TABLE 4
Linear regression analysis of the $M_{\rm BH} - M_{*,\rm sph}$ diagram.

Subsample (size)	Regression	α	β	$\langle M_{*,\rm sph}\rangle$	ϵ	Δ
	$\log[M_{\rm BH}/{\rm M}_\odot] = \alpha + \beta\log[(M_{*,\rm sph} - \langle M_{*,\rm sph}\rangle)/{\rm M}_\odot]$					
Core-Sérsic (22)	BCES $(Y\|X)$	9.06 ± 0.09	0.86 ± 0.28	11.28	–	0.42
	BCES $(X\|Y)$	9.06 ± 0.12	1.70 ± 0.32	11.28	–	0.61
	BCES Bisector	9.06 ± 0.10	1.19 ± 0.23	11.28	–	0.47
	FITEXY $(Y\|X)$	$9.06^{+0.08}_{-0.08}$	$0.68^{+0.21}_{-0.20}$	11.28	$0.36^{+0.09}_{-0.06}$	0.42
	FITEXY $(X\|Y)$	$9.03^{+0.15}_{-0.16}$	$1.90^{+0.85}_{-0.46}$	11.28	$0.62^{+0.13}_{-0.10}$	0.68
	FITEXY Bisector	$9.05^{+0.12}_{-0.13}$	$1.12^{+0.35}_{-0.27}$	11.28	–	0.46
	`linmix_err` $(Y\|X)$	9.04 ± 0.10	0.64 ± 0.25	11.28	0.40 ± 0.09	0.42
	`linmix_err` $(X\|Y)$	9.03 ± 0.17	1.80 ± 0.70	11.28	0.67 ± 0.30	0.65
	`linmix_err` Bisector	9.04 ± 0.14	1.06 ± 0.35	11.28	–	0.45
Sérsic (44)	BCES $(Y\|X)$	7.71 ± 0.09	0.95 ± 0.21	10.25	–	0.64
	BCES $(X\|Y)$	7.71 ± 0.16	2.52 ± 0.54	10.25	–	1.11
	BCES Bisector	7.71 ± 0.11	1.48 ± 0.20	10.25	–	0.74
	FITEXY $(Y\|X)$	$7.72^{+0.10}_{-0.09}$	$0.96^{+0.21}_{-0.21}$	10.25	$0.58^{+0.09}_{-0.07}$	0.64
	FITEXY $(X\|Y)$	$7.72^{+0.16}_{-0.16}$	$2.49^{+0.69}_{-0.45}$	10.25	$0.93^{+0.15}_{-0.13}$	1.10
	FITEXY Bisector	$7.72^{+0.13}_{-0.13}$	$1.49^{+0.33}_{-0.28}$	10.25	–	0.74
	`linmix_err` $(Y\|X)$	7.73 ± 0.10	0.98 ± 0.24	10.25	0.59 ± 0.08	0.65
	`linmix_err` $(X\|Y)$	7.73 ± 0.17	2.48 ± 0.59	10.25	0.95 ± 0.27	1.10
	`linmix_err` Bisector	7.73 ± 0.14	1.49 ± 0.57	10.25	–	0.74
Early-type (E+S0) (45)	BCES $(Y\|X)$	8.56 ± 0.07	0.85 ± 0.12	10.81	–	0.48
	BCES $(X\|Y)$	8.56 ± 0.09	1.27 ± 0.13	10.81	–	0.59
	BCES Bisector	$\mathbf{8.56 \pm 0.07}$	$\mathbf{1.04 \pm 0.10}$	**10.81**	–	**0.51**
	mFITEXY $(Y\|X)$	$8.56^{+0.06}_{-0.07}$	$0.83^{+0.11}_{-0.11}$	10.81	$0.42^{+0.07}_{-0.05}$	0.48
	mFITEXY $(X\|Y)$	$8.54^{+0.08}_{-0.09}$	$1.32^{+0.18}_{-0.15}$	10.81	$0.53^{+0.08}_{-0.07}$	0.61
	mFITEXY Bisector	$8.55^{+0.07}_{-0.08}$	$1.05^{+0.14}_{-0.12}$	10.81	–	0.51
	`linmix_err` $(Y\|X)$	8.55 ± 0.07	0.82 ± 0.12	10.81	0.43 ± 0.06	0.48
	`linmix_err` $(X\|Y)$	8.55 ± 0.09	1.29 ± 0.17	10.81	0.54 ± 0.11	0.59
	`linmix_err` Bisector	8.55 ± 0.08	1.03 ± 0.19	10.81	–	0.51
Late-type (Sp) (17)	BCES $(Y\|X)$	7.18 ± 0.17	1.95 ± 1.52	10.05	–	0.74
	BCES $(X\|Y)$	7.18 ± 0.39	5.89 ± 3.40	10.05	–	1.70
	BCES Bisector	$\mathbf{7.18 \pm 0.21}$	$\mathbf{3.00 \pm 1.30}$	**10.05**	–	**0.94**
	mFITEXY $(Y\|X)$	$7.20^{+0.15}_{-0.16}$	$1.22^{+0.70}_{-0.62}$	10.05	$0.59^{+0.16}_{-0.11}$	0.66
	mFITEXY $(X\|Y)$	$7.44^{+1.45}_{-0.52}$	$7.14^{+26.31}_{-3.01}$	10.05	$1.49^{+0.56}_{-0.36}$	2.08
	mFITEXY Bisector	$\mathbf{7.24^{+1.04}_{-0.39}}$	$\mathbf{2.28^{+1.67}_{-1.01}}$	**10.05**	–	**0.79**
	`linmix_err` $(Y\|X)$	7.23 ± 0.19	0.96 ± 0.96	10.05	0.67 ± 0.16	0.65
	`linmix_err` $(X\|Y)$	7.42 ± 0.64	6.96 ± 6.73	10.05	1.83 ± 1.86	2.03
	`linmix_err` Bisector	7.26 ± 0.47	1.94 ± 216.38	10.05	–	0.74

Note. — For each subsample, we indicate $\langle M_{*,\rm sph}\rangle$, its average value of spheroid stellar masses. In the last two columns, we report ϵ, the intrinsic scatter, and Δ, the total rms scatter in the $\log(M_{\rm BH})$ direction.

tion. The BCES routine (Akritas & Bershady 1996) was run via the python module written by Rodrigo Nemmen (Nemmen et al. 2012), which is available at https://github.com/rsnemmen/BCES.

REFERENCES

Akritas, M. G., & Bershady, M. A. 1996, ApJ, 470, 706
Arnold, J. A., Romanowsky, A. J., Brodie, J. P., et al. 2014, ApJ, 791, 80
Athanassoula, E. 2005, MNRAS, 358, 1477
Balcells, M., Graham, A. W., & Peletier, R. F. 2007, ApJ, 665, 1104
Bardeen, J. M. 1975, in IAU Symposium, Vol. 69, Dynamics of the Solar Systems, ed. A. Hayli, 297
Beifiori, A., Courteau, S., Corsini, E. M., & Zhu, Y. 2012, MNRAS, 419, 2497
Bekki, K. 2010, MNRAS, 401, L58
Chilingarian, I. V., Cayatte, V., Durret, F., et al. 2008, A&A, 486, 85
Cody, A. M., Carter, D., Bridges, T. J., Mobasher, B., & Poggianti, B. M. 2009, MNRAS, 396, 1647
Combes, F., Debbasch, F., Friedli, D., & Pfenniger, D. 1990, A&A, 233, 82
Combes, F., & Sanders, R. H. 1981, A&A, 96, 164
Davies, J. I., Phillipps, S., Cawson, M. G. M., Disney, M. J., & Kibblewhite, E. J. 1988, MNRAS, 232, 239
Davies, R. L., Efstathiou, G., Fall, S. M., Illingworth, G., & Schechter, P. L. 1983, ApJ, 266, 41
de Rijcke, S., Michielsen, D., Dejonghe, H., Zeilinger, W. W., & Hau, G. K. T. 2005, A&A, 438, 491
dos Anjos, S., & da Silva, M. B. 2013, Memorie della Societa Astronomica Italiana Supplementi, 25, 33
Dressler, A. 1989, in IAU Symposium, Vol. 134, Active Galactic Nuclei, ed. D. E. Osterbrock & J. S. Miller, 217
Dullo, B. T., & Graham, A. W. 2014, MNRAS, 444, 2700
Eliche-Moral, M. C., González-García, A. C., Balcells, M., et al. 2011, A&A, 533, A104
Emsellem, , & E. et al. 2011, MNRAS, 414, 888
Erwin, P., Beltrán, J. C. V., Graham, A. W., & Beckman, J. E. 2003, ApJ, 597, 929
Erwin, P., & Gadotti, D. A. 2012, Advances in Astronomy, 2012, 4
Erwin, P., Saglia, R., Thomas, J., et al. 2015, in IAU Symposium, Vol. 309, IAU Symposium, ed. B. L. Ziegler, F. Combes, H. Dannerbauer, & M. Verdugo, 359–360
Fazio, G. G., Hora, J. L., Allen, L. E., et al. 2004, ApJS, 154, 10
Ferrarese, L., & Ford, H. 2005, Space Sci. Rev., 116, 523
Ferrarese, L., & Merritt, D. 2000, ApJ, 539, L9
Forbes, D. A., Lasky, P., Graham, A. W., & Spitler, L. 2008, MNRAS, 389, 1924
Gadotti, D. A. 2009, MNRAS, 393, 1531

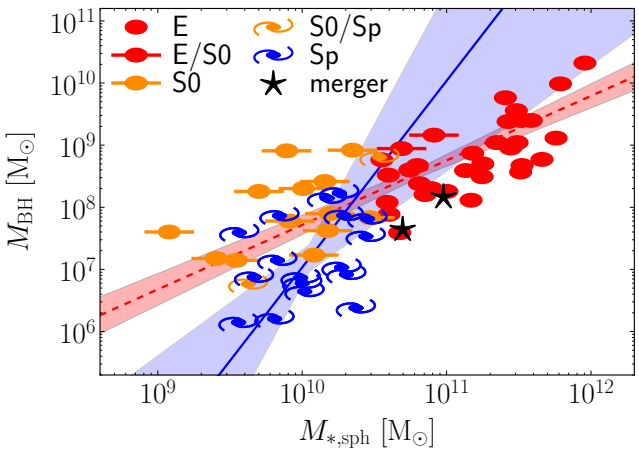

FIG. 5.— Black hole mass plotted against spheroid stellar mass. Symbols are coded according to the galaxy morphological type. The red dashed line indicates the BCES bisector linear regression for the bulges of the 45 early-type galaxies (E+S0), with the red shaded area denoting its 1σ uncertainty. The bulges of early-type galaxies follow $M_{\rm BH} \propto M_{*,\rm sph}^{1.04\pm0.10}$, a near-linear relation consistent with a dry-merging formation scenario. The steeper blue solid line shows the BCES bisector linear regression for the bulges of the 17 late-type (Sp) galaxies, with the blue shaded area denoting its 1σ uncertainty. The bulges of late-type galaxies follow $M_{\rm BH} \propto M_{*,\rm sph}^{2-3}$, indicating that gas-rich processes feed the black hole more efficiently ("quadratically" or "cubically") than the host bulge grows in stellar mass. We note that AGNs with $10^5 \lesssim M_{\rm BH}/{\rm M}_\odot \lesssim 2\times10^6$ (Jiang et al. 2011) appear to follow the blue line (see Graham et al. 2015, *in preparation*).

Gavazzi, G., Boselli, A., Donati, A., Franzetti, P., & Scodeggio, M. 2003, A&A, 400, 451
Gebhardt, K., Bender, R., Bower, G., et al. 2000, ApJ, 539, L13
Graham, A. 2015a, Highlights of Astronomy, 16, 360
Graham, A. W. 2007, MNRAS, 379, 711
—. 2012, ApJ, 746, 113
—. 2013, Elliptical and Disk Galaxy Structure and Modern Scaling Laws, ed. T. D. Oswalt & W. C. Keel, 91
Graham, A. W. 2014, in Astronomical Society of the Pacific Conference Series, Vol. 480, Structure and Dynamics of Disk Galaxies, ed. M. S. Seigar & P. Treuthardt, 185
—. 2015b, ArXiv e-prints, arXiv:1501.02937
—. 2015c, ArXiv e-prints, arXiv:1501.02937
Graham, A. W., Erwin, P., Trujillo, I., & Asensio Ramos, A. 2003, AJ, 125, 2951
Graham, A. W., & Guzmán, R. 2003, AJ, 125, 2936
Graham, A. W., Onken, C. A., Athanassoula, E., & Combes, F. 2011, MNRAS, 412, 2211
Graham, A. W., & Scott, N. 2013, ApJ, 764, 151
—. 2015, ApJ, 798, 54
Graham, A. W., & Worley, C. C. 2008, MNRAS, 388, 1708
Gültekin, K., Richstone, D. O., Gebhardt, K., et al. 2009, ApJ, 698, 198
Häring, N., & Rix, H.-W. 2004, ApJ, 604, L89
Held, E. V., de Zeeuw, T., Mould, J., & Picard, A. 1992, in IAU Symposium, Vol. 149, The Stellar Populations of Galaxies, ed. B. Barbuy & A. Renzini, 429
Hohl, F. 1975, in IAU Symposium, Vol. 69, Dynamics of the Solar Systems, ed. A. Hayli, 349
Jerjen, H., Binggeli, B., & Freeman, K. C. 2000, AJ, 119, 593
Jiang, N., Ho, L. C., Dong, X.-B., Yang, H., & Wang, J. 2013, ApJ, 770, 3
Jiang, Y.-F., Greene, J. E., & Ho, L. C. 2011, ApJ, 737, L45
Kelly, B. C. 2007, ApJ, 665, 1489
Keselman, J. A., & Nusser, A. 2012, MNRAS, 424, 1232
Kormendy, J. 2015, ArXiv e-prints, arXiv:1504.03330
Kormendy, J., & Ho, L. C. 2013, ARA&A, 51, 511
Kormendy, J., & Richstone, D. 1995, ARA&A, 33, 581
Kourkchi, E., Khosroshahi, H. G., Carter, D., et al. 2012, MNRAS, 420, 2819
Laor, A. 1998, ApJ, 505, L83
—. 2001, ApJ, 553, 677
Läsker, R., Ferrarese, L., & van de Ven, G. 2014a, ApJ, 780, 69
Läsker, R., Ferrarese, L., van de Ven, G., & Shankar, F. 2014b, ApJ, 780, 70
Lauer, T. R., Faber, S. M., Richstone, D., et al. 2007a, ApJ, 662, 808
—. 2007b, ApJ, 662, 808
Liu, F. S., Xia, X. Y., Mao, S., Wu, H., & Deng, Z. G. 2008, MNRAS, 385, 23
MacArthur, L. A., González, J. J., & Courteau, S. 2009, MNRAS, 395, 28
Magorrian, J., Tremaine, S., Richstone, D., et al. 1998, AJ, 115, 2285
Malumuth, E. M., & Kirshner, R. P. 1981, ApJ, 251, 508
Marconi, A., & Hunt, L. K. 2003, ApJ, 589, L21
Mathur, S., Fields, D., Peterson, B. M., & Grupe, D. 2012, ApJ, 754, 146
Matković, A., & Guzmán, R. 2005, MNRAS, 362, 289
McConnell, N. J., & Ma, C.-P. 2013, ApJ, 764, 184
McConnell, N. J., Ma, C.-P., Gebhardt, K., et al. 2011, Nature, 480, 215
Meidt, S. E., Schinnerer, E., van de Ven, G., et al. 2014, ApJ, 788, 144
Nemmen, R. S., Georganopoulos, M., Guiriec, S., et al. 2012, Science, 338, 1445
Peletier, R. F., Kutdemir, E., van der Wolk, G., et al. 2012, MNRAS, 419, 2031
Pfenniger, D., & Friedli, D. 1991, A&A, 252, 75
Press, W. H., Teukolsky, S. A., Vetterling, W. T., & Flannery, B. P. 1992, Numerical recipes in FORTRAN. The art of scientific computing
Querejeta, M., Eliche-Moral, M. C., Tapia, T., et al. 2015, A&A, 573, A78
Reines, A. E., Greene, J. E., & Geha, M. 2013, ApJ, 775, 116
Rusli, S. P., Thomas, J., Saglia, R. P., et al. 2013, AJ, 146, 45
Ryan, C. J., De Robertis, M. M., Virani, S., Laor, A., & Dawson, P. C. 2007, ApJ, 654, 799
Saha, K., Martinez-Valpuesta, I., & Gerhard, O. 2012, MNRAS, 421, 333
Sani, E., Marconi, A., Hunt, L. K., & Risaliti, G. 2011, MNRAS, 413, 1479
Savorgnan, G. A. D., & Graham, A. W. 2015, MNRAS, 446, 2330
Scannapieco, C., White, S. D. M., Springel, V., & Tissera, P. B. 2011, MNRAS, 417, 154
Schechter, P. L. 1980, AJ, 85, 801
Scott, N., Davies, R. L., Houghton, R. C. W., et al. 2014, MNRAS, 441, 274
Scott, N., Graham, A. W., & Schombert, J. 2013, ApJ, 768, 76
Seidel, M. K., Cacho, R., Ruiz-Lara, T., et al. 2015, MNRAS, 446, 2837
Sheth, K., Regan, M., Hinz, J. L., et al. 2010, PASP, 122, 1397
Tortora, C., Napolitano, N. R., Romanowsky, A. J., Capaccioli, M., & Covone, G. 2009, MNRAS, 396, 1132
Tremaine, S., Gebhardt, K., Bender, R., et al. 2002, ApJ, 574, 740
Trujillo, I., Erwin, P., Asensio Ramos, A., & Graham, A. W. 2004, AJ, 127, 1917
van den Bosch, R. C. E., Gebhardt, K., Gültekin, K., et al. 2012, Nature, 491, 729
Vika, M., Driver, S. P., Cameron, E., Kelvin, L., & Robotham, A. 2012, MNRAS, 419, 2264
von der Linden, A., Best, P. N., Kauffmann, G., & White, S. D. M. 2007, MNRAS, 379, 867
Wandel, A. 1999, ApJ, 519, L39
Yee, H. K. C. 1992, in Astronomical Society of the Pacific Conference Series, Vol. 31, Relationships Between Active Galactic Nuclei and Starburst Galaxies, ed. A. V. Filippenko, 417
Young, C. K., & Currie, M. J. 1994, MNRAS, 268, L11